

A hybridizable discontinuous Galerkin method for the Navier–Stokes equations with pointwise divergence-free velocity field

Sander Rhebergen^{a,1}, Garth N. Wells^{b,2}

^a*Department of Applied Mathematics, University of Waterloo, Waterloo N2L 3G1, Canada*

^b*Department of Engineering, University of Cambridge, Trumpington Street, Cambridge CB2 1PX, United Kingdom*

Abstract

We introduce a hybridizable discontinuous Galerkin method for the incompressible Navier–Stokes equations for which the approximate velocity field is pointwise divergence-free. The method proposed here builds on the method presented by Labeur and Wells [SIAM J. Sci. Comput., vol. 34 (2012), pp. A889–A913]. We show that with simple modifications of the function spaces in the method of Labeur and Wells that it is possible to formulate a simple method with pointwise divergence-free velocity fields, and which is both momentum conserving and energy stable. Theoretical results are verified by two- and three-dimensional numerical examples and for different orders of polynomial approximation.

Keywords: Navier–Stokes equations, hybridized, discontinuous Galerkin, finite element methods, solenoidal.

1. Introduction

Numerous finite element methods for the incompressible Navier–Stokes equations result in approximate velocity fields that are not pointwise divergence-free. This lack of pointwise satisfaction of the continuity equation typically leads to violation of conservation laws beyond just mass conservation, such as conservation of energy. A key issue is that, in the absence of a pointwise solenoidal velocity field, the conservative and advective format of the Navier–Stokes equations are not equivalent. The review paper by John et al. [1] presents cases for the Stokes limit where the lack of pointwise enforcement of the continuity equation can lead to large errors. Elements that are stable (in sense of the inf-sup condition), but do not enforce the continuity equation pointwise, such as

Email addresses: srheberg@uwaterloo.ca (Sander Rhebergen), gnw20@cam.ac.uk (Garth N. Wells)

¹ORCID: 0000-0001-6036-0356

²ORCID: 0000-0001-5291-7951

the Taylor–Hood, Crouzeix–Raviart, and MINI elements, can suffer from large errors in the pressure which in turn can pollute the velocity approximation. The concept of ‘pressure-robustness’ to explain the aforementioned issues is discussed by John et al. [1]. A second issue is when a computed velocity field that is not pointwise divergence-free is used as the advective velocity in a transport solver. The lack of pointwise incompressibility can lead to spurious results and can compromise stability of the transport equation.

Discontinuous Galerkin (DG) finite element methods provide a natural framework for handling the advective term in the Navier–Stokes equations, and have been studied extensively in this context, e.g. [2, 3, 4, 5, 6, 7]. A difficulty in the construction of DG methods for the Navier–Stokes equations is that it is not possible to have both an energy-stable *and* locally momentum conserving method unless the approximate velocity is exactly divergence-free [3, p. 1068]. To overcome this problem, a post-processing operator was introduced by Cockburn et al. [3]. The operator, which is a slight modification of the Brezzi–Douglas–Marini interpolation operator (see e.g. [8]), when applied to the DG approximate velocity field provides a post-processed approximate velocity that is pointwise divergence-free. Key to this operator is that it can be applied element-wise and is therefore inexpensive to apply. A second issue with DG methods, and a common criticism, is that the number of degrees-of-freedom on a given mesh is considerably larger than for a conforming method. This is especially the case in three dimensions.

An approach to generating pointwise divergence-free velocity fields is to use a $H(\text{div})$ -conforming velocity field, in which the normal component of the velocity is continuous across facets, together with a discontinuous pressure field from an appropriate space. Such a velocity space can be constructed by using a $H(\text{div})$ -conforming finite element space, or by enforcing the desired continuity via hybridization [8]. However, construction of $H(\text{div})$ -conforming methods is not straightforward as the tangential components of the viscous stress on cell facets must be appropriately handled. Moreover, for advection dominated flows it is not immediately clear how the advective terms can be appropriately stabilised. Examples of hybridization for the Stokes equations can be found in [9, 10, 11], and in Navier–Stokes equations [12].

A synthesis of discontinuous Galerkin and hybridized methods has led to the development of hybridizable Discontinuous Galerkin (HDG) finite element methods [13, 14]. These methods were introduced with the purpose of reducing the computational cost of DG methods on a given mesh. This is achieved as follows. Approximate variables and their numerical fluxes across element boundaries are expressed in terms of approximate traces of the variables on facets. By coupling the degrees of freedom on an element only with degrees of freedom of approximate trace variables, element degrees of freedom can be eliminated in favour of facet degrees of freedom only. The result is that the HDG global system of algebraic equations is significantly smaller than those obtained using DG.

It has been shown that, after post-processing, solutions obtained by HDG methods may show super-convergence results for elliptic problems (for polyno-

mial approximations of order k , the order of accuracy is order $k + 2$). This property has been exploited also in the context of the Navier–Stokes equations by, e.g., [15, 16]. Although their velocity field is not automatically pointwise divergence-free, they introduce a post-processing that not only results in an approximate velocity field that is exactly divergence-free and $H(\text{div})$ -conforming, but also a velocity field that super-converges for low Reynolds number flows. Super-convergence is, however, lost when the flow is convection dominated.

In this paper we use the HDG approach to construct a simple discretization of the Navier–Stokes equations in which the approximate velocity field is $H(\text{div})$ -conforming and pointwise divergence-free. To achieve this, we first note that unlike many other HDG methods for incompressible flows [15, 17, 18, 12, 19, 16, 20], the HDG methods of Labeur and Wells [21] and Rhebergen and Cockburn [22] contain also facet unknowns for the pressure. The element pressure unknowns play the role of cell-wise Lagrange multiplier to enforce the continuity, whereas the facet pressure unknowns play the role of Lagrange multipliers enforcing continuity of the normal component of the velocity across cell boundaries. It was shown already in [21] that if the polynomial approximation of the element pressure on simplices is one order lower than the polynomial approximation of the element velocity, that the approximate velocity field is exactly divergence-free element-wise. However, they were unable to obtain $H(\text{div})$ -conforming function spaces, because their facet pressure approximation spaces were not rich enough to enforce normal continuity of the velocity across element boundaries exactly. A consequence was that while the method satisfied the continuity equation exactly, it could not satisfy both momentum conservation and energy stability simultaneously. We show in sections 3.2 and 3.3 that if this facet pressure space is chosen rich enough we obtain approximate velocity fields that are $H(\text{div})$ -conforming and exactly divergence-free on the whole domain. A consequence is that the HDG method introduced here exactly conserves mass, momentum and is energy stable.

The remainder of this paper is organized as follows. Section 2 briefly introduces the Navier–Stokes problem, which is followed by the main result of this paper in section 3; a momentum conserving and energy stable HDG method for the Navier–Stokes equations with pointwise solenoidal velocity field. Numerical results are presented in section 4 and conclusions are drawn in section 5.

2. Incompressible Navier–Stokes problem

Let $\Omega \subset \mathbb{R}^d$ be a polygonal ($d = 2$) or polyhedral ($d = 3$) domain with boundary outward unit normal n , and let the time interval of interest be given by $I = (0, t_N]$. Given the kinematic viscosity $\nu \in \mathbb{R}^+$ and forcing term $f : \Omega \times I \rightarrow \mathbb{R}^d$, the Navier–Stokes equations for the velocity field $u : \Omega \times I \rightarrow \mathbb{R}^d$ and kinematic pressure field $p : \Omega \times I \rightarrow \mathbb{R}$ are given by

$$\partial_t u + \nabla \cdot \sigma = f \quad \text{in } \Omega \times I, \quad (1a)$$

$$\nabla \cdot u = 0 \quad \text{in } \Omega \times I, \quad (1b)$$

where σ is the momentum flux:

$$\sigma := \sigma_a + \sigma_d \quad \text{with} \quad \sigma_a := u \otimes u \quad \text{and} \quad \sigma_d := p\mathbb{I} - \nu \nabla u, \quad (2)$$

and \mathbb{I} is the identity tensor and $(a \otimes b)_{ij} = a_i b_j$.

We partition the boundary of Ω such that $\partial\Omega = \Gamma_D \cup \Gamma_N$ and $\Gamma_D \cap \Gamma_N = \emptyset$. Given $h : \Gamma_N \times I \rightarrow \mathbb{R}^d$ and a solenoidal initial velocity field $u_0 : \Omega \rightarrow \mathbb{R}^d$, we prescribe the following boundary and initial conditions:

$$u = 0 \quad \text{on } \Gamma_D \times I, \quad (3a)$$

$$\sigma \cdot n - \max(u \cdot n, 0) u = h \quad \text{on } \Gamma_N \times I, \quad (3b)$$

$$u(x, 0) = u_0(x) \quad \text{in } \Omega. \quad (3c)$$

On inflow parts of Γ_N ($u \cdot n < 0$) we impose the total momentum flux, i.e., $\sigma \cdot n = h$. On outflow parts of Γ_N ($u \cdot n \geq 0$), only the diffusive part of the momentum flux is prescribed, i.e., $\sigma_d \cdot n = h$.

Equation (1a) is the conservative form of the Navier–Stokes equation. With satisfaction of the incompressibility constraint, eq. (1b), the momentum equation (1a) can be equivalently expressed as:

$$\partial_t u + (1 - \chi)u \cdot \nabla u + \chi \nabla \cdot \sigma_a + \nabla \cdot \sigma_d = f, \quad (4)$$

where $\chi \in [0, 1]$. For numerous finite element methods, the approximate velocity field is not pointwise or locally (in a weak sense) solenoidal. In such cases, it can be shown that momentum is conserved if $\chi = 1$, while energy stability can be proven if $\chi = 1/2$. For stabilised finite element methods in which the continuity equation is not satisfied locally, manipulations of the advective term can be applied to achieve momentum conservation [23].

The hybridizable discontinuous Galerkin method of Labeur and Wells [21] is based on a weak formulation of eq. (4) with $\chi = 1/2$. It thereby gives up momentum conservation in favour of energy stability. We will show how the method of Labeur and Wells [21] can be formulated to satisfy the continuity equation pointwise. As a consequence, on the discrete level eq. (4) is unchanging for all values of χ . We will show that this leads to a method that is both energy stable and momentum conserving.

3. A hybridizable discontinuous Galerkin method

We present a hybridizable discontinuous Galerkin method for the Navier–Stokes problem for which the approximate velocity field is pointwise divergence-free.

3.1. Preliminaries

Let $\mathcal{T} := \{K\}$ be a triangulation of the domain Ω into non-overlapping simplex cells K . The boundary of a cell is denoted by ∂K and the outward unit normal vector on ∂K by n . Two adjacent cells K^+ and K^- share an

interior facet $F := \overline{\partial K^+} \cap \overline{\partial K^-}$. A facet of ∂K that lies on the boundary of the domain $\partial\Omega$ is called a boundary facet. The sets of interior and boundary facets are denoted by \mathcal{F}_I and \mathcal{F}_B , respectively. The set of all facets is denoted by $\mathcal{F} := \mathcal{F}_I \cup \mathcal{F}_B$.

3.2. Semi-discrete formulation

Consider the following finite element spaces:

$$V_h := \left\{ v_h \in [L^2(\mathcal{T})]^d, v_h \in [P_k(K)]^d \quad \forall K \in \mathcal{T} \right\}, \quad (5a)$$

$$\bar{V}_h := \left\{ \bar{v}_h \in [L^2(\mathcal{F})]^d, \bar{v}_h \in [P_k(F)]^d \quad \forall F \in \mathcal{F}, \bar{v}_h = 0 \text{ on } \Gamma_D \right\}, \quad (5b)$$

$$Q_h := \left\{ q_h \in L^2(\mathcal{T}), q_h \in P_{k-1}(K) \quad \forall K \in \mathcal{T} \right\}, \quad (5c)$$

$$\bar{Q}_h := \left\{ \bar{q}_h \in L^2(\mathcal{F}), \bar{q}_h \in P_k(F) \quad \forall F \in \mathcal{F} \right\}, \quad (5d)$$

where $P_l(D)$ denotes the space of polynomials of degree $l > 0$ on a domain D . Note that the spaces V_h and Q_h are defined on the whole domain \mathcal{T} , whereas the spaces \bar{V}_h and \bar{Q}_h are defined only on facets of the triangulation.

The spaces V_h and Q_h are discontinuous across cell boundaries, hence the trace of a function $a \in V_h$ may be double-valued on cell boundaries. At an interior facet, F , we denote the traces of $a \in V_h$ by a^+ and a^- . We introduce the jump operator $[[a]] := a^+ \cdot n^+ + a^- \cdot n^-$, where n^\pm the outward unit normal on ∂K^\pm .

We now state the weak formulation of the proposed method: given a forcing term $f \in [L^2(\Omega)]^d$, boundary condition $h \in [L^2(\Gamma_N)]^d$ and viscosity ν , find $u_h, \bar{u}_h, p_h, \bar{p}_h \in V_h \times \bar{V}_h \times Q_h \times \bar{Q}_h$ such that:

$$0 = \sum_K \int_K u_h \cdot \nabla q_h \, dx - \sum_K \int_{\partial K} u_h \cdot n q_h \, ds \quad \forall q_h \in Q_h, \quad (6a)$$

$$0 = \sum_K \int_{\partial K} u_h \cdot n \bar{q}_h \, ds - \int_{\partial\Omega} \bar{u}_h \cdot n \bar{q}_h \, ds \quad \forall \bar{q}_h \in \bar{Q}_h, \quad (6b)$$

and

$$\begin{aligned} \int_{\Omega} f \cdot v_h \, dx &= \int_{\Omega} \partial_t u_h \cdot v_h \, dx - \sum_K \int_K \sigma_h : \nabla v_h \, dx + \sum_K \int_{\partial K} \hat{\sigma}_h : (v_h \otimes n) \, ds \\ &\quad + \sum_K \int_{\partial K} \nu ((\bar{u}_h - u_h) \otimes n) : \nabla v_h \, ds \quad \forall v_h \in V_h, \end{aligned} \quad (6c)$$

$$\int_{\Gamma_N} h \cdot \bar{v}_h \, ds = \sum_K \int_{\partial K} \hat{\sigma}_h : (\bar{v}_h \otimes n) \, ds - \int_{\Gamma_N} (1 - \lambda) (\bar{u}_h \cdot n) \bar{u}_h \cdot \bar{v}_h \, ds \quad \forall \bar{v}_h \in \bar{V}_h, \quad (6d)$$

where $\hat{\sigma}_h := \hat{\sigma}_{a,h} + \hat{\sigma}_{d,h}$ is the ‘numerical flux’ on cell facets. The advective part of the numerical flux is given by:

$$\hat{\sigma}_{a,h} := \sigma_a + (\bar{u}_h - u_h) \otimes \lambda u_h, \quad (7)$$

where λ is an indicator function that takes on a value of unity on inflow cell boundaries (where $u_h \cdot n < 0$) and a value of zero on outflow cell facets (where $u_h \cdot n \geq 0$). This definition of the numerical flux provides upwinding of the advective component of the flux. The diffusive part of the numerical flux is defined as

$$\hat{\sigma}_{d,h} := \bar{p}_h \mathbb{I} - \nu \nabla u_h - \frac{\nu \alpha}{h_K} (\bar{u}_h - u_h) \otimes n, \quad (8)$$

where $\alpha > 0$ is a penalty parameter as is typical of Nitsche and interior penalty methods. It is proven in [24, 25] that α needs to be sufficiently large to ensure stability.

A key feature of this formulation, and what distinguishes it from standard discontinuous Galerkin methods, is that functions on cells (functions in V_h and Q_h) are not coupled across facets directly via the numerical flux. Rather, fields on neighbouring cells are coupled via the facet functions \bar{u}_h and \bar{p}_h . The fields u_h and p_h can therefore be eliminated locally via static condensation, resulting in a global system of equations in terms of the facet functions only. This substantially reduces the size of the global systems compared to a standard discontinuous Galerkin method on the same mesh.

The weak formulation presented here is the weak formulation of Labour and Wells [21] with conservative form of the advection term ($\chi = 1$ in eq. (4)). The key difference is that we have been more prescriptive on the relationships between the finite element spaces in eq. (5), and this leads to some appealing properties, as we will prove. In particular, the spaces in eq. (5) are such that: for $u_h \in [P_k(K)]^d$, $\nabla \cdot u_h \in P_{k-1}(K)$ and $u_h \cdot n \in P_k(F)$; and for $\bar{u}_h \in [P_k(F)]^d$, $\bar{u}_h \cdot n \in P_k(F)$. Furthermore, the function spaces have been chosen such that the resulting method is inf-sup stable, see [25]. The resulting weak formulation can be shown to be equivalent to a weak formulation in which the approximate velocity field lies in the Brezzi–Douglas–Marini (BDM) finite element space. Hybridization of other $H(\text{div})$ conforming finite element spaces, see e.g. [8], are also possible.

Proposition 1 (mass conservation). *If $u_h \in V_h$ and $\bar{u}_h \in \bar{V}_h$ satisfy eq. (6), with V_h and \bar{V}_h defined in eq. (5), then*

$$\nabla \cdot u_h = 0 \quad \forall x \in K, \forall K \in \mathcal{T}, \quad (9)$$

and

$$\llbracket u_h \rrbracket = 0 \quad \forall x \in F, \forall F \in \mathcal{F}_I, \quad (10a)$$

$$u_h \cdot n = \bar{u}_h \cdot n \quad \forall x \in F, \forall F \in \mathcal{F}_B. \quad (10b)$$

Proof. Applying integration-by-parts to eq. (6a):

$$0 = \int_K q_h \nabla \cdot u_h \, dx \quad \forall q_h \in P_{k-1}(K), \forall K \in \mathcal{T}. \quad (11)$$

Since $q_h, \nabla \cdot u_h \in P_{k-1}(K)$, pointwise satisfaction of the continuity equation, eq. (9), follows.

It follows from eq. (6b) that:

$$0 = \sum_{F \in \mathcal{F}_I} \int_F \llbracket u_h \rrbracket \bar{q}_h \, ds + \sum_{F \in \mathcal{F}_B} \int_F (u_h - \bar{u}_h) \cdot n \bar{q}_h \, ds \quad \forall \bar{q}_h \in \bar{Q}_h. \quad (12)$$

Since $\bar{q}_h, u_h \cdot n, \bar{u}_h \cdot n \in P_k(F)$, eq. (10) follows. \square

Proposition 1 is a stronger statement of mass conservation than in Labour and Wells [21, Proposition 4.2], in which mass conservation was proved locally (cell-wise) in an integral sense only. Under certain conditions, implementations in [21] satisfy eq. (9), but not eq. (10). We will show that this difference is critical for the new formulation in this work as it allows simultaneous satisfaction of momentum conservation and energy stability.

We next show momentum conservation for the semi-discrete weak formulation in terms of the numerical flux.

Proposition 2 (momentum conservation). *Let $u_h, \bar{u}_h, p_h, \bar{p}_h \in V_h \times \bar{V}_h \times Q_h \times \bar{Q}_h$ satisfy eq. (6). Then,*

$$\frac{d}{dt} \int_K u_h \, dx = \int_K f \, dx - \int_{\partial K} \hat{\sigma}_h n \, ds \quad \forall K \in \mathcal{T}. \quad (13)$$

Furthermore, if $\Gamma_D = \emptyset$,

$$\frac{d}{dt} \int_{\Omega} u_h \, dx = \int_{\Omega} f \, dx - \int_{\partial\Omega} (1 - \lambda)(\bar{u}_h \cdot n) \bar{u}_h \, ds - \int_{\partial\Omega} h \, ds. \quad (14)$$

Proof. In eq. (6c), set $v_h = e_j$ on K , where e_j is a canonical unit basis vector, and set $v_h = 0$ on $\mathcal{T} \setminus K$ in eq. (6c):

$$\frac{d}{dt} \int_K u_h \cdot e_j \, dx + \int_{\partial K} (\hat{\sigma}_h \cdot n) \cdot e_j \, ds = \int_K f \cdot e_j \, dx, \quad (15)$$

which proves eq. (13). Equation (14) follows immediately by setting $v_h = e_j$ in eq. (6c), $\bar{v}_h = -e_j$ in eq. (6d) and summing the two results. \square

We next prove that the method is *also* globally energy stable.

Proposition 3 (global energy stability). *If $u_h, \bar{u}_h, p_h, \bar{p}_h \in V_h \times \bar{V}_h \times Q_h \times \bar{Q}_h$ satisfy eq. (6), for homogeneous boundary conditions, $f = 0$ and for a suitably large α :*

$$\frac{d}{dt} \sum_K \int_K |u_h|^2 \, dx \leq 0. \quad (16)$$

Proof. Setting $q_h = -p_h$, $\bar{q}_h = -\bar{p}_h$, $v_h = \bar{u}_h$ and $\bar{v}_h = -\bar{u}_h$ in eqs. (6a) to (6d) and inserting the expressions for the numerical fluxes (eqs. (2), (7) and (8)), and summing:

$$\begin{aligned}
& \sum_K \frac{1}{2} \int_K \partial_t |u_h|^2 dx + \sum_K \frac{1}{2} \int_{\partial K} (u_h \cdot n) |u_h|^2 ds \\
& \quad - \sum_K \frac{1}{2} \int_{\partial K} (u_h \cdot n) |\bar{u}_h|^2 ds + \sum_K \frac{1}{2} \int_{\partial K} |u_h \cdot n| |u_h - \bar{u}_h|^2 ds \\
& \quad + \sum_K \int_K \nu |\nabla u_h|^2 dx + \sum_K \int_{\partial K} \frac{\nu \alpha}{h_K} |\bar{u}_h - u_h|^2 ds \\
& + 2 \sum_K \int_{\partial K} \nu (\nabla u_h \cdot n) \cdot (\bar{u}_h - u_h) ds + \int_{\Gamma_N} (1 - \lambda) (\bar{u}_h \cdot n) |\bar{u}_h|^2 ds \\
& \quad - \sum_K \int_K (u_h \otimes u_h) : \nabla u_h dx = 0, \quad (17)
\end{aligned}$$

where we have used that $\lambda u_h \cdot n = (u_h \cdot n - |u_h \cdot n|) / 2$, and applied integration-by-parts to the pressure gradient terms. Since \bar{u}_h is single-valued on facets, the normal component of u_h is continuous across facets and $\bar{u}_h \cdot n = u_h \cdot n$ on the domain boundary (see proposition 1), the third integral on the left-hand side of eq. (17) can be simplified:

$$- \sum_K \frac{1}{2} \int_{\partial K} (u_h \cdot n) |\bar{u}_h|^2 ds = -\frac{1}{2} \int_{\Gamma_N} (\bar{u}_h \cdot n) |\bar{u}_h|^2 ds. \quad (18)$$

We consider now the last term on the left-hand side of eq. (17). On each cell K it holds that $-u_h \otimes u_h : \nabla u_h = (\nabla \cdot u_h)(u_h \cdot u_h) / 2 - \nabla \cdot ((u_h \otimes u_h) \cdot u_h) / 2 = -\nabla \cdot ((u_h \otimes u_h) \cdot u_h) / 2$, since $\nabla \cdot u_h = 0$ (by proposition 1). It follows that

$$- \sum_K \int_K (u_h \otimes u_h) : \nabla u_h dx = -\frac{1}{2} \sum_K \int_{\partial K} (u_h \cdot n) |u_h|^2 ds. \quad (19)$$

Combining eqs. (17) to (19),

$$\begin{aligned}
& \frac{1}{2} \sum_K \int_K \partial_t |u_h|^2 dx = -\frac{1}{2} \sum_K \int_{\partial K} |u_h \cdot n| |u_h - \bar{u}_h|^2 ds \\
& \quad - \sum_K \int_K \nu |\nabla u_h|^2 dx - \sum_K \int_{\partial K} \frac{\nu \alpha}{h_K} |\bar{u}_h - u_h|^2 ds \\
& \quad - 2 \sum_K \int_{\partial K} \nu (\nabla u_h \cdot n) \cdot (\bar{u}_h - u_h) ds - \frac{1}{2} \int_{\Gamma_N} |\bar{u}_h \cdot n| |\bar{u}_h|^2 ds, \quad (20)
\end{aligned}$$

where we have used that

$$\int_{\Gamma_N} (1 - \lambda) (\bar{u}_h \cdot n) |\bar{u}_h|^2 ds - \frac{1}{2} \int_{\Gamma_N} (\bar{u}_h \cdot n) |\bar{u}_h|^2 ds = \frac{1}{2} \int_{\Gamma_N} |\bar{u}_h \cdot n| |\bar{u}_h|^2 ds. \quad (21)$$

It can be proven that there exists an $\alpha > 0$, independent of h_K , such that

$$\sum_K \int_{\partial K} \frac{\nu \alpha}{h_K} |\bar{u}_h - u_h|^2 ds \geq 2 \left| \sum_K \int_{\partial K} \nu (\nabla u_h \cdot n) \cdot (\bar{u}_h - u_h) ds \right|, \quad (22)$$

(see [24, Lemma 5.2] and [25, Lemma 2]). Therefore, the right-hand side of eq. (20) is non-positive, proving eq. (16). \square

The keys to be able to prove global energy stability for this conservative form of the Navier–Stokes equations are: (a) the pointwise solenoidal velocity field; and (b) continuity of the normal component of the velocity field across facets. The latter point was not fulfilled by the method in [21].

3.3. A fully-discrete weak formulation

We now consider a fully-discrete formulation. We partition the time interval I into an ordered series of time levels $0 = t^0 < t^1 < \dots < t^N$. The difference between each time level is denoted by $\Delta t^n = t^{n+1} - t^n$. To discretize in time, we consider the θ -method and denote midpoint values of a function y by $y^{n+\theta} := (1-\theta)y^n + \theta y^{n+1}$. Following Labeur and Wells [21], the convective velocity will be evaluated at the current time t^n , thereby linearizing the problem, i.e.:

$$\sigma_h^{n+\theta} = \sigma_{a,h}^{n+\theta} + \sigma_{d,h}^{n+\theta} \quad \text{where} \quad \sigma_{a,h}^{n+\theta} = u_h^{n+\theta} \otimes u_h^n, \quad (23)$$

and

$$\hat{\sigma}_h^{n+\theta} = \hat{\sigma}_{a,h}^{n+\theta} + \hat{\sigma}_{d,h}^{n+\theta} \quad \text{where} \quad \hat{\sigma}_{a,h}^{n+\theta} = \sigma_{a,h}^{n+\theta} + (\bar{u}_h^{n+\theta} - u_h^{n+\theta}) \otimes \lambda u_h^n. \quad (24)$$

The time-discrete counterpart of eq. (6) is: given $u_h^n, \bar{u}_h^n, p_h^n, \bar{p}_h^n \in V_h \times \bar{V}_h \times Q_h \times \bar{Q}_h$ at time t^n , the forcing term $f^{n+\theta} \in [L^2(\Omega)]^d$, the boundary condition $h^{n+\theta} \in [L^2(\Gamma_N)]^d$, and the viscosity ν , find $u_h^{n+1}, \bar{u}_h^{n+1}, p_h^{n+1}, \bar{p}_h^{n+1} \in V_h \times \bar{V}_h \times Q_h \times \bar{Q}_h$ such that mass conservation,

$$0 = \sum_K \int_K u_h^{n+1} \cdot \nabla q_h dx - \sum_K \int_{\partial K} u_h^{n+1} \cdot n q_h ds, \quad (25a)$$

$$0 = \sum_K \int_{\partial K} u_h^{n+1} \cdot n \bar{q}_h ds - \int_{\partial \Omega} \bar{u}_h^{n+1} \cdot n \bar{q}_h ds, \quad (25b)$$

and momentum conservation,

$$\begin{aligned} \int_{\Omega} f^{n+\theta} \cdot v_h dx &= \int_{\Omega} \frac{u_h^{n+1} - u_h^n}{\Delta t^n} \cdot v_h dx - \sum_K \int_K \sigma_h^{n+\theta} : \nabla v_h dx \\ &\quad + \sum_K \int_{\partial K} \hat{\sigma}_h^{n+\theta} : v_h \otimes n ds \\ &\quad + \sum_K \int_{\partial K} \nu \left((\bar{u}_h^{n+\theta} - u_h^{n+\theta}) \otimes n \right) : \nabla v_h ds, \end{aligned} \quad (25c)$$

$$\int_{\Gamma_N} h^{n+\theta} \cdot \bar{v}_h \, ds = \sum_K \int_{\partial K} \hat{\sigma}_h^{n+\theta} : \bar{v}_h \otimes n \, ds - \int_{\Gamma_N} (1-\lambda) (\bar{u}_h^n \cdot n) \bar{u}_h^{n+\theta} \cdot \bar{v}_h \, ds, \quad (25d)$$

are satisfied for all $v_h, \bar{v}_h, q_h, \bar{q}_h \in V_h \times \bar{V}_h \times Q_h \times \bar{Q}_h$. Here λ is evaluated using the known velocity field at time t^n .

In section 3.2 we proved that the semi-discrete formulation eq. (6) is momentum conserving, energy stable and exactly mass conserving when using the function spaces given by eq. (5). We show next that the fully-discrete formulation given by eq. (25) inherits these properties.

Proposition 4 (fully-discrete mass conservation). *If $u_h^{n+1} \in V_h$ and $\bar{u}_h^{n+1} \in \bar{V}_h$ satisfy eq. (25), then*

$$\nabla \cdot u_h^{n+1} = 0 \quad \forall x \in K, \forall K \in \mathcal{T}, \quad (26)$$

and

$$\llbracket u_h^{n+1} \rrbracket = 0 \quad \forall x \in \mathcal{F}, \forall \mathcal{F} \in \mathcal{F}_I, \quad (27a)$$

$$u_h^{n+1} \cdot n = \bar{u}_h^{n+1} \cdot n \quad \forall x \in \mathcal{F}, \forall \mathcal{F} \in \mathcal{F}_B. \quad (27b)$$

Proof. The proof is similar to that of proposition 1 and therefore omitted. \square

Proposition 5 (fully-discrete momentum conservation). *If $u_h^n, \bar{u}_h^n, p_h^n, \bar{p}_h^n \in V_h \times \bar{V}_h \times Q_h \times \bar{Q}_h$ and $u_h^{n+1}, \bar{u}_h^{n+1}, p_h^{n+1}, \bar{p}_h^{n+1} \in V_h \times \bar{V}_h \times Q_h \times \bar{Q}_h$ satisfy eq. (25), then*

$$\int_K \frac{u_h^{n+1} - u_h^n}{\Delta t^n} \, dx = \int_K f^{n+\theta} \, dx - \int_{\partial K} \hat{\sigma}_h^{n+\theta} n \, ds \quad \forall K \in \mathcal{T}. \quad (28)$$

Furthermore, if $\Gamma_D = \emptyset$,

$$\sum_K \int_K \frac{u_h^{n+1} - u_h^n}{\Delta t^n} \, dx = \sum_K \int_K f^{n+\theta} \, dx - \int_{\partial \Omega} (1-\lambda) (\bar{u}_h^n \cdot n) \bar{u}_h^{n+\theta} \, ds - \int_{\partial \Omega} h^{n+\theta} \, ds. \quad (29)$$

Proof. The proof is similar to that of proposition 2 and therefore omitted. \square

Proposition 6 (fully-discrete energy stability). *If $u_h^n, \bar{u}_h^n, p_h^n, \bar{p}_h^n \in V_h \times \bar{V}_h \times Q_h \times \bar{Q}_h$ and $u_h^{n+1}, \bar{u}_h^{n+1}, p_h^{n+1}, \bar{p}_h^{n+1} \in V_h \times \bar{V}_h \times Q_h \times \bar{Q}_h$ satisfy eq. (25), then with homogeneous boundary conditions, no forcing terms, for suitably large α , and $\theta \geq 1/2$,*

$$\sum_K \int_K |u_h^{n+1}|^2 \, dx \leq \sum_K \int_K |u_h^n|^2 \, dx. \quad (30)$$

Proof. Setting $q_h = -\theta p_h^{n+\theta}$, $\bar{q}_h = -\theta \bar{p}_h^{n+\theta}$, $v_h = u_h^{n+\theta}$ and $\bar{v}_h = -\bar{u}_h^{n+\theta}$, in eqs. (25a) to (25d), adding the results, using the expressions for the diffusive fluxes, given by eqs. (2) and (8), partial integration of the pressure gradient terms and using that $\nabla \cdot u_h^n = 0$ by proposition 4, we obtain, using the same steps as in the proof of proposition 3,

$$\begin{aligned} & \int_{\Omega} \frac{u_h^{n+1} - u_h^n}{\Delta t^n} \cdot u_h^{n+\theta} \, dx + \sum_K \frac{1}{2} \int_{\partial K} |u_h^n \cdot n| |u_h^{n+\theta} - \bar{u}_h^{n+\theta}|^2 \, ds \\ & \quad + \sum_K \int_K \nu |\nabla u_h^{n+\theta}|^2 \, dx + \sum_K \int_{\partial K} \frac{\nu \alpha}{h_K} |\bar{u}_h^{n+\theta} - u_h^{n+\theta}|^2 \, ds \\ & \quad + 2 \sum_K \int_{\partial K} \nu (\nabla u_h^{n+\theta} \cdot n) (\bar{u}_h^{n+\theta} - u_h^{n+\theta}) \, ds \\ & \quad + \frac{1}{2} \int_{\Gamma_N} |\bar{u}_h^n \cdot n| |\bar{u}_h^{n+\theta}|^2 \, ds = 0. \quad (31) \end{aligned}$$

The first term on the left-hand side of eq. (31) can be reformulated as

$$\begin{aligned} \int_{\Omega} \frac{u_h^{n+1} - u_h^n}{\Delta t^n} \cdot u_h^{n+\theta} \, dx &= \left(\theta - \frac{1}{2} \right) \int_{\Omega} \frac{|u_h^{n+1} - u_h^n|^2}{\Delta t^n} \, dx \\ & \quad + \frac{1}{2} \int_{\Omega} \frac{|u_h^{n+1}|^2}{\Delta t^n} \, dx - \frac{1}{2} \int_{\Omega} \frac{|u_h^n|^2}{\Delta t^n} \, dx. \quad (32) \end{aligned}$$

Inserting this expression into eq. (31):

$$\begin{aligned} & \frac{1}{2} \int_{\Omega} \frac{|u_h^{n+1}|^2}{\Delta t^n} \, dx - \frac{1}{2} \int_{\Omega} \frac{|u_h^n|^2}{\Delta t^n} \, dx = - \left(\theta - \frac{1}{2} \right) \int_{\Omega} \frac{|u_h^{n+1} - u_h^n|^2}{\Delta t^n} \, dx \\ & \quad - \sum_K \frac{1}{2} \int_{\partial K} |u_h^n \cdot n| |u_h^{n+\theta} - \bar{u}_h^{n+\theta}|^2 \, ds \\ & \quad - 2 \sum_K \int_{\partial K} \nu (\nabla u_h^{n+\theta} \cdot n) (\bar{u}_h^{n+\theta} - u_h^{n+\theta}) \, ds \\ & \quad - \sum_K \int_{\partial K} \frac{\nu \alpha}{h_K} |\bar{u}_h^{n+\theta} - u_h^{n+\theta}|^2 \, ds \\ & \quad - \frac{1}{2} \int_{\Gamma_N} |\bar{u}_h^n \cdot n| |\bar{u}_h^{n+\theta}|^2 \, ds - \sum_K \int_K \nu |\nabla u_h^{n+\theta}|^2 \, dx. \quad (33) \end{aligned}$$

As in proposition 3, there exists an $\alpha > 0$, independent of h_K , such that the right hand side of eq. (33) is non-positive. The result follows. \square

4. Numerical examples

We now demonstrate the performance of the method for a selection of numerical examples, paying close attention to mass and momentum conservation,

and energy stability.

For all stationary examples considered, exact solutions are known. For the stationary examples we use a fixed-point iteration with stopping criterion $|e_p^{i+1} - e_p^i| / (e_p^{i+1} + e_p^i) \leq \text{TOL}$, where e_p^i is the pressure error in the L^2 norm at the i th iterate, and TOL is a given tolerance that we set to 10^{-4} . All unsteady examples use $\theta = 1$. In all examples we set the penalty parameter to be $\alpha = 6k^2$.

In the implementation we apply cell-wise static condensation such that only the degrees-of-freedom associated with the facet spaces appear in the global system. Compared to standard discontinuous Galerkin methods, this significantly reduces the size of the global system. It is possible to reduce the size of the global system even further by taking into account that velocity is continuous in the normal direction and therefore we could remove the normal components from \bar{V}_h , see [12]. In the current paper, however, we only apply static condensation. The examples have been implemented using the NGSolve finite element library [26]. All examples use unstructured simplicial meshes.

4.1. Kovaszny flow

We consider the steady, two-dimensional analytical solution of the Navier-Stokes equations from Kovaszny [27] on a domain $\Omega = (-0.5, 1) \times (-0.5, 1.5)$. For a Reynolds number Re , let the viscosity be given by $\nu = 1/Re$. The solution to the Kovaszny problem is:

$$u_x = 1 - e^{\lambda x_1} \cos(2\pi x_2), \quad (34a)$$

$$u_y = \frac{\lambda}{2\pi} e^{\lambda x_1} \sin(2\pi x_2), \quad (34b)$$

$$p = \frac{1}{2} (1 - e^{2\lambda x_1}) + C, \quad (34c)$$

where C is an arbitrary constant, and where

$$\lambda = \frac{Re}{2} - \left(\frac{Re^2}{4} + 4\pi^2 \right)^{1/2} \quad (35)$$

We choose C such that the mean pressure on Ω is zero. The Kovaszny flow solution in eq. (34) is used to set Dirichlet boundary conditions for the velocity on $\partial\Omega$.

The L^2 -error and rates of convergence are presented in table 1 for $Re = 40$ using a series of refined meshes. Optimal rates of convergence are observed for both the velocity field (order $k+1$) and pressure field (order k). The divergence of the approximate velocity field is of machine precision in all cases.

4.2. Position-dependent Coriolis force

We now consider the test case from [28, Section 3.2]. In particular, we consider on the unit square $(0, 1) \times (0, 1)$ the steady Navier-Stokes equations augmented with a position-dependent Coriolis force: $\nabla \cdot \sigma + 2C \times u = 0$ and

Table 1: Computed velocity, pressure and divergence errors in the L^2 norm for the HDG method applied to the Kovaszny problem.

Cells	$k = 2$				
	$\ u_h - u\ $	rate	$\ p_h - p\ $	rate	$\ \nabla \cdot u_h\ $
64	1.8e-2	-	1.6e-2	-	3.8e-14
256	2.2e-3	3.0	4.0e-3	2.0	6.7e-14
1024	2.8e-4	3.0	9.8e-4	2.0	1.3e-13
4096	3.5e-5	3.0	2.4e-4	2.0	2.5e-13

Cells	$k = 3$				
	$\ u_h - u\ $	rate	$\ p_h - p\ $	rate	$\ \nabla \cdot u_h\ $
64	1.4e-3	-	2.0e-3	-	1.9e-13
256	9.4e-5	3.9	2.0e-4	3.3	6.1e-13
1024	5.8e-6	4.0	2.3e-5	3.1	7.8e-13
4096	3.6e-7	4.0	2.8e-6	3.1	1.6e-12

Table 2: Computed errors in the L^2 norm for the HDG method with the position-dependent Coriolis forcing term with different viscosity values.

Cells	$\nu = 0.001, k = 2$				$\nu = 1, k = 2$			
	$\ u_h - u\ $	$\ \nabla \cdot u_h\ $	$\ p_h - p\ $	rate	$\ u_h - u\ $	$\ \nabla \cdot u_h\ $	$\ p_h - p\ $	rate
64	3.7e-15	4.6e-14	9.0e-4	-	1.3e-14	4.6e-14	9.0e-4	-
256	5.1e-15	9.3e-14	2.3e-4	2.0	9.9e-15	9.2e-14	2.3e-4	2.0
1024	6.4e-15	1.8e-13	5.6e-5	2.0	7.8e-14	1.9e-13	5.6e-5	2.0
4096	2.2e-14	6.3e-13	1.4e-5	2.0	2.3e-13	3.7e-13	1.4e-5	2.0

$\nabla \cdot u = 0$, where we set $2C \times u = -2x_2(-u_2, u_1)$ and $\nu = 1$. On boundaries we set $u = (1, 0)$. The exact solution to this problem is given by $p = x_2^2 - 1/3$ and $u = (1, 0)$.

It was shown in [28] that the Scott–Vogelius finite element, in which the velocity is approximated in divergence-free function spaces, is able to produce the exact velocity field while the velocity computed using a Taylor–Hood finite element method is polluted by the pressure error, in part due to the approximate velocity field not being exactly divergence-free. Furthermore, it is shown in [28] that as $\nu \rightarrow 0$, the velocity error increases for the Taylor–Hood finite element method. In table 2 we show the results obtained using the HDG method presented in section 3 for $k = 2$.

Table 2 shows the computed error in the L^2 norm for the velocity, pressure and divergence errors. Errors in the velocity and velocity divergence are of machine precision, regardless of ν . The HDG method therefore obtains the same quality of solution as produced using the Scott–Vogelius finite element in [28]. We do not consider the $k = 3$ case because for this discretization the pressure is approximated by quadratic polynomials and so the pressure error is also of machine precision.

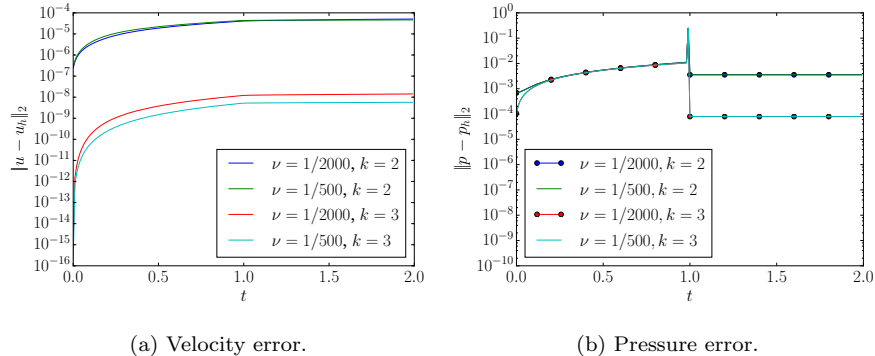


Figure 1: Velocity and pressure errors for the transient higher-order potential flow test case. Approximations were obtained using $k = 2$ and $k = 3$ on a mesh with 2048 cells.

4.3. Transient higher-order potential flow

In this test, taken from [29, Section 6.6], we solve the time dependent Navier–Stokes equations eq. (1) on the domain $\Omega = [-1, 1]^2$. This test case studies the time-dependent exact velocity $u(t) = \min(t, 1)\nabla\chi$ where χ is a smooth harmonic potential given by $\chi = x_1^3x_2 - x_2^3x_1$. The pressure gradient then satisfies $\nabla p = -\nabla|u|^2/2 - \partial_t(\min(t, 1)\nabla\chi)$. We impose the exact velocity solution as Dirichlet boundary condition on all of $\partial\Omega$.

For the simulations we used a grid with 2048 cells, set the time step equal to $\Delta t = 0.01$ and compute the solution on the time interval $[0, 2]$. Figure 1 shows the velocity and pressure errors as a function of time. We used both $k = 2$ and $k = 3$, and consider $\nu = 1/500$ and $\nu = 1/2000$. We observe that the error in pressure and velocity is more or less the same regardless of ν .

Over the computational time interval, using $k = 2$ or $k = 3$ on a mesh with 2048 cells, for either $\nu = 1/500$ and $\nu = 1/2000$, the L^2 -norm of the divergence reaches 1.4×10^{-10} in one point but is otherwise always of the order 10^{-11} . The momentum balance, in absolute value, never exceeds 3.4×10^{-12} .

4.4. Two-dimensional flow past a circular obstacle

In this test case we consider flow past a circular obstacle (see e.g. [12, 30]). The domain is a rectangular channel, $[0, 2.2] \times [0, 0.41]$, with a circular obstacle of radius $r = 0.05$ centred at $(0.2, 0.2)$. On the inflow boundary ($x_1 = 0$) we prescribe the x_1 -component of the velocity to be $u_1 = 6x_2(0.41 - x_2)/0.41^2$. The x_2 -component of the velocity is prescribed as $u_2 = 0$. Homogeneous Dirichlet boundary conditions are applied on the walls ($x_2 = 0$ and $x_2 = 0.41$), and on the obstacle. On the outflow boundary ($x_1 = 2.2$) we prescribe $\sigma_d \cdot n = 0$. The viscosity is set as $\nu = 10^{-3}$. We choose $k = 3$ and set $\Delta t = 5 \times 10^{-5}$ so that the spatial discretization error dominates the temporal discretization error. For the initial condition, we impose the steady Stokes solution of this problem. The mesh of the domain has 6784 cells and we consider the time interval $[0, 5]$.

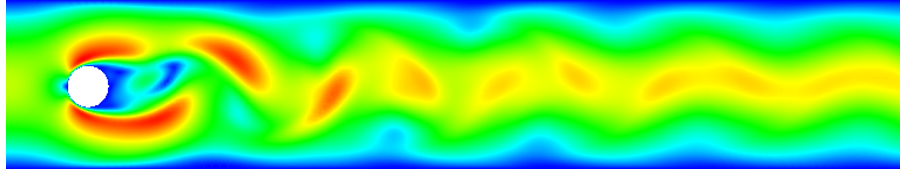


Figure 2: Two-dimensional flow past a cylinder test case: velocity magnitude past a two-dimensional circular object in a channel at $t = 5$. Approximations were obtained using $k = 3$ on a mesh with 6784 cells.

At each time step we compute the drag and lift coefficients, which are defined as

$$C_D = -\frac{1}{r} \int_{\Gamma_c} (\sigma_d \cdot n) \cdot e_1 \, ds, \quad C_L = -\frac{1}{r} \int_{\Gamma_c} (\sigma_d \cdot n) \cdot e_2 \, ds, \quad (36)$$

where e_1 and e_2 are unit vectors in the x_1 and x_2 directions, respectively, and Γ_C is the surface of the circular object. We compute a maximum drag coefficient of $C_D = 3.23232$ and minimum drag coefficient of $C_D = 3.16583$. The maximum and minimum lift coefficients we compute are, respectively, $C_L = 0.98251$ and $C_L = -1.02246$. These are comparable to those found in literature [12, 30]. The velocity magnitude at $t = 5$ is shown fig. 2.

4.5. Three-dimensional flow past a cylinder

In this test case we consider three-dimensional flow past a cylinder (see e.g. [12, 30]) with a time dependent inflow velocity. The domain is a cuboid shaped channel $[0, 2.5] \times [0, 0.41] \times [0, 0.41]$ with a cylinder of radius $r_{\text{cyl}} = 0.05$ around the x_3 -axis centred at $(x_1, x_2) = (0.5, 0.2)$. On the inflow boundary ($x_1 = 0$) we prescribe the x_1 -component of the velocity to be $u_1 = 36 \sin(\pi t/8) x_2 x_3 (0.41 - x_2)(0.41 - x_3)/0.41^4$. The x_2 - and x_3 -components of the velocity are prescribed as $u_2 = 0$ and $u_3 = 0$. We impose homogeneous Dirichlet boundary conditions on the walls ($x_2 = 0$, $x_2 = 0.41$, $x_3 = 0$ and $x_3 = 0.41$) and on the cylinder. On the outflow boundary ($x_1 = 2.5$) we prescribe $\sigma_d \cdot n = 0$. The viscosity is set as $\nu = 10^{-3}$.

We choose $k = 3$ and set $\Delta t = 5 \times 10^{-4}$ so that the spatial discretization error dominates the temporal discretization error. The initial condition is the Stokes solution to this problem. The mesh has 4091 cells and we compute on the time interval $[0, 8]$. At each time step we compute the drag and lift coefficients, defined by eq. (36), where $r = 0.41 r_{\text{cyl}}$ and Γ_C is the surface of the cylinder. We compute maximum drag and lift coefficients of $C_D = 2.98815$ and $C_L = 0.00348$, respectively. Compared to Schäfer et al. [30], in which the maximum drag and lift coefficients lie in the intervals $C_D \in [3.2000, 3.3000]$ and $C_L \in [0.0020, 0.0040]$, we slightly under-predict the drag coefficient, but the lift coefficient lies within the same interval. Figure 3 shows the velocity magnitude at $t = 4$.

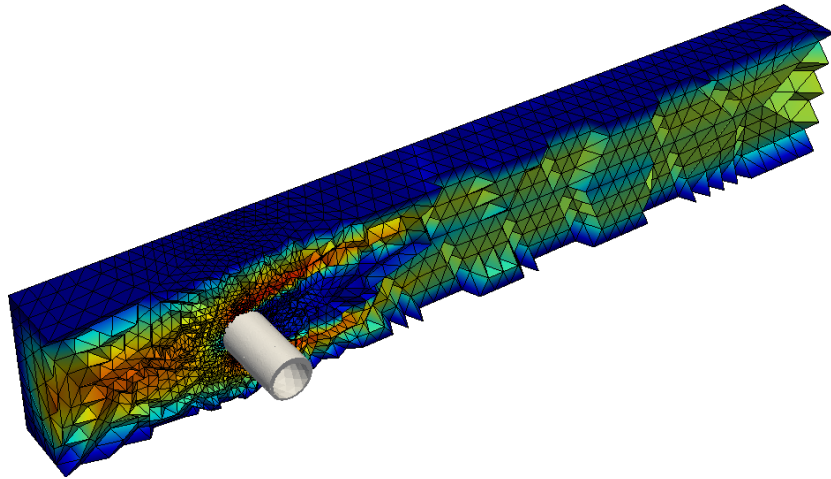


Figure 3: Three-dimensional flow past a cylinder test: slice through a 3D channel showing the 3D velocity magnitude past a cylinder in a channel at $t = 4$. Approximations were obtained using $k = 3$ on a mesh with 4091 cells.

5. Conclusions

We have introduced a formulation of a hybridizable discontinuous Galerkin method for the incompressible Navier–Stokes equations that computes velocity fields that are pointwise divergence-free. The construction of solenoidal velocity fields does not require post-processing or the use of finite dimensional spaces of divergence-free functions. The pointwise satisfaction of the continuity equation and the continuity of the normal component of the velocity field across cell facets allows us to prove that the method conserves momentum locally (cell-wise) and is energy stable. This is in contrast with the closely related method in Labeur and Wells [21] which can satisfy local momentum conservation or global energy stability, but not both simultaneously. The analysis that we present is supported by a range of numerical examples in two and three dimensions.

Acknowledgements

SR gratefully acknowledges support from the Natural Sciences and Engineering Research Council of Canada through the Discovery Grant program (RGPIN-05606-2015) and the Discovery Accelerator Supplement (RGPAS-478018-2015).

References

References

- [1] V. John, A. Linke, C. Merdon, M. Neilan, L. G. Rebholz, On the divergence constraint in mixed finite element methods for incompressible flows, SIAM Review URL http://www.wias-berlin.de/preprint/2177/wias_preprints_2177.pdf, to appear.

- [2] F. Bassi, A. Crivellini, D. A. Di Pietro, S. Rebay, An artificial compressibility flux for the discontinuous Galerkin solution of the incompressible Navier–Stokes equations, *J. Comput. Phys.* 218 (2) (2006) 794–815, URL <http://dx.doi.org/10.1016/j.jcp.2006.03.006>.
- [3] B. Cockburn, G. Kanschat, D. Schötzau, A locally conservative LDG method for the incompressible Navier–Stokes equations, *Math. Comp.* 74 (251) (2004) 1067–1095, URL <http://dx.doi.org/10.1090/S0025-5718-04-01718-1>.
- [4] E. Ferrer, R. H. J. Willden, A high order discontinuous Galerkin finite element solver for the incompressible Navier–Stokes equations, *Comput. Fluids* 46 (2011) 224–240, URL <http://dx.doi.org/10.1016/j.compfluid.2010.10.018>.
- [5] D. A. Di Pietro, A. Ern, *Mathematical Aspects of Discontinuous Galerkin Methods*, vol. 69 of *Mathématiques et Applications*, Springer–Verlag Berlin Heidelberg, 2012.
- [6] S. Rhebergen, B. Cockburn, J. J. W. van der Vegt, A space–time discontinuous Galerkin method for the incompressible Navier–Stokes equations, *J. Comput. Phys.* 233 (15) (2013) 339–358, URL <http://dx.doi.org/10.1016/j.jcp.2012.08.052>.
- [7] K. Shahbazi, P. F. Fischer, C. R. Ethier, A high-order discontinuous Galerkin method for the unsteady incompressible Navier–Stokes equations, *J. Comput. Phys.* 222 (1) (2007) 391–407, URL <http://dx.doi.org/10.1016/j.jcp.2006.07.029>.
- [8] D. Boffi, F. Brezzi, M. Fortin, *Mixed Finite Element Methods and Applications*, vol. 44 of *Springer Series in Computational Mathematics*, Springer–Verlag Berlin Heidelberg, 2013.
- [9] J. Carrero, B. Cockburn, D. Schötzau, Hybridized globally divergence-free LDG methods. Part I: the Stokes problem, *Math. Comp.* 75 (254), URL <http://dx.doi.org/10.1090/S0025-5718-05-01804-1>.
- [10] B. Cockburn, J. Gopalakrishnan, Incompressible finite elements via hybridization. Part I: the Stokes system in two space dimensions, *SIAM J. Numer. Anal.* 43 (4) (2005) 1627–1650, URL <http://dx.doi.org/10.1137/04061060X>.
- [11] B. Cockburn, J. Gopalakrishnan, Incompressible finite elements via hybridization. Part II: the Stokes system in three space dimensions, *SIAM J. Numer. Anal.* 43 (4) (2005) 1651–1672, URL <http://dx.doi.org/10.1137/040610659>.
- [12] C. Lehrenfeld, J. Schöberl, High order exactly divergence-free hybrid discontinuous Galerkin Methods for unsteady incompressible flows, *Comput.*

- Methods Appl. Mech. Engrg. 307 (2016) 339–361, URL <http://dx.doi.org/10.1016/j.cma.2016.04.025>.
- [13] R. J. Labeur, G. N. Wells, A Galerkin interface stabilisation method for the advection–diffusion and incompressible Navier–Stokes equations, *Comput Methods Appl Mech Engrg* 196 (49–52) (2007) 4985–5000, URL <http://dx.doi.org/10.1016/j.cma.2007.06.025>.
- [14] B. Cockburn, J. Gopalakrishnan, R. Lazarov, Unified hybridization of discontinuous Galerkin, mixed, and continuous Galerkin methods for second order elliptic problems, *SIAM J Numer Anal* 47 (2) (2009) 1319–1365, URL <http://dx.doi.org/10.1137/070706616>.
- [15] A. Cesmelioglu, B. Cockburn, W. Qiu, Analysis of a hybridizable discontinuous Galerkin method for the steady-state incompressible Navier–Stokes equations, *Math. Comp.* URL <https://doi.org/10.1090/mcom/3195>.
- [16] N. C. Nguyen, J. Peraire, B. Cockburn, An implicit high–order hybridizable discontinuous Galerkin method for the incompressible Navier–Stokes equations, *J. Comput. Phys.* 230 (4) (2011) 1147–1170, URL <http://dx.doi.org/10.1016/j.jcp.2010.10.032>.
- [17] B. Cockburn, J. Gopalakrishnan, The derivation of hybridizable discontinuous Galerkin methods for Stokes equations, *SIAM J. Numer. Anal.* 47 (2) (2009) 1092–1125, URL <http://dx.doi.org/10.1137/080726653>.
- [18] B. Cockburn, J. Gopalakrishnan, N. C. Nguyen, J. Peraire, F. J. Sayas, Analysis of HDG methods for Stokes flow, *Math. Comp.* 80 (274) (2011) 723–760, URL <http://dx.doi.org/10.1090/S0025-5718-2010-02410-X>.
- [19] N. C. Nguyen, J. Peraire, B. Cockburn, A hybridizable discontinuous Galerkin method for Stokes flow, *Comput. Methods Appl. Mech. Engrg.* 199 (9–12) (2010) 582–597, URL <http://dx.doi.org/10.1016/j.cma.2009.10.007>.
- [20] W. Qiu, K. Shi, A superconvergent HDG method for the incompressible Navier–Stokes equations on general polyhedral meshes, *IMA J. Numer. Anal.* 36 (4) (2016) 1943–1967, URL <http://dx.doi.org/10.1093/imanum/drv067>.
- [21] R. J. Labeur, G. N. Wells, Energy stable and momentum conserving hybrid finite element method for the incompressible Navier–Stokes equations, *SIAM J Sci Comput* 34 (2) (2012) A889–A913, URL <http://dx.doi.org/10.1137/100818583>.
- [22] S. Rhebergen, B. Cockburn, A space-time hybridizable discontinuous Galerkin method for incompressible flows on deforming domains, *J. Comput. Phys.* 231 (11) (2012) 4185–4204, URL <http://dx.doi.org/10.1016/j.jcp.2012.02.011>.

- [23] T. J. R. Hughes, G. N. Wells, Conservation properties for the Galerkin and stabilised forms of the advection-diffusion and incompressible Navier–Stokes equations, *Comput Methods Appl Mech Engrg* 194 (9–11) (2005) 1141–1159, URL <http://dx.doi.org/10.1016/j.cma.2004.06.034>.
- [24] G. N. Wells, Analysis of an interface stabilized finite element method: the advection-diffusion-reaction equation, *SIAM J. Numer. Anal.* 49 (1) (2011) 87–109, URL <http://dx.doi.org/10.1137/090775464>.
- [25] S. Rhebergen, G. N. Wells, Analysis of a hybridized/interface stabilized finite element method for the Stokes equations, URL <https://arxiv.org/abs/1607.02118>, 2016.
- [26] J. Schöberl, C++11 Implementation of Finite Elements in NGSolve, Tech. Rep. ASC Report 30/2014, Institute for Analysis and Scientific Computing, Vienna University of Technology, URL <http://www.asc.tuwien.ac.at/~schoeberl/wiki/publications/ngs-cpp11.pdf>, 2014.
- [27] L. I. G. Kovasznay, Laminar flow behind a two-dimensional grid, *Proc. Cambridge Philos. Soc.* 44 (1948) 58–62, URL <https://doi.org/10.1017/S0305004100023999>.
- [28] A. Linke, C. Merdon, On velocity errors due to irrotational forces in the Navier–Stokes momentum balance, *J. Comput. Phys.* 313 (2016) 654–661, URL <http://dx.doi.org/10.1016/j.jcp.2016.02.070>.
- [29] A. Linke, C. Merdon, Pressure-robustness and discrete Helmholtz projectors in mixed finite element methods for the incompressible Navier–Stokes equations, *Comput. Methods Appl. Mech. Engrg.* URL <http://dx.doi.org/10.1016/j.cma.2016.08.018>.
- [30] M. Schäfer, S. Turek, F. Durst, E. Krause, R. Rannacher, Benchmark computations of laminar flow around a cylinder, in: E. H. Hirschel (Ed.), *Flow Simulation with High-Performance Computers II*, 547–566, 1996.